

Empirical Scaling Laws for Truck Bomb Explosions Based on Seismic and Acoustic Data

by Keith D. Koper,* Terry C. Wallace, Robert E. Reinke, and John A. Leverette

Abstract We analyze seismic and acoustic data from a series of controlled truck bomb explosions to develop scaling laws and functional relations between charge size and various waveform properties. The explosions had yields of $3\text{--}12 \times 10^3$ kg trinitrotoluene (TNT), and the receivers were placed at distances of 1–16 km, so the data mimic the data previously recorded from actual terrorist truck bombings. We examine four airblast properties (peak overpressure, impulse per unit area, pulse duration, and average shock velocity) and three seismic properties (peak displacement of P wave, low-frequency asymptote of displacement spectrum, and the corner frequency of displacement spectrum) as potential yield estimators. Impulse per unit area and pulse duration observations prove to be the most robust yield indicators; however, peak overpressure, peak displacement, and low-frequency spectral asymptote have significant utility as well. The acoustic scaling laws are more portable than the seismic scaling laws because regional differences in atmospheric structure can be well described by pressure and temperature observations, while regional differences in geologic structure are dependent on a large number of less accessible parameters. We apply the scaling laws developed here to seismic waveforms of the 1998 Nairobi bombing and find a yield of $2.0\text{--}6.0 \times 10^3$ kg TNT. This value is consistent with but more precise than a previous estimate made via a time domain waveform inversion. Additional testing indicates that our functional relations are likely applicable to surface chemical explosions in general and not limited solely to truck bombs.

Introduction

Broadband seismometers are most often deployed to record ground motion generated by earthquakes or to monitor underground nuclear testing. However, as the number of permanently installed instruments continues to grow, it is becoming common to record so-called exotic sources. Examples of exotic sources that have recently been studied seismically include supersonic aircraft (Kanamori *et al.*, 1991), bolides (Chael and Spalding, 1996), rockfalls (Uhrhammer, 1996), geysers (Kedar *et al.*, 1996), mine collapses (Pechmann *et al.*, 1995; Yang *et al.*, 1998), quarry blasts (Barker *et al.*, 1997), industrial explosions (Ichinose *et al.*, 1999), aircraft crashes (McCormack *et al.*, 1999), and terrorist bombings (Holzer *et al.*, 1996; Koper *et al.*, 1999).

Numerous exotic-source observations have also been made using instruments that record variations in atmospheric pressure. Classic examples include barometric recordings of the Krakatoa volcanic eruption of 1883 and the Siberian bolide of 1908, while more recent examples include infrasonic

detections of a bolide above northern Germany (Evers and Haak, 2001), a pipeline explosion in southern New Mexico (B. Stump, 2001, written comm.), and the explosion of a Dutch warehouse containing fireworks (Evers and Haak, 2000). The current renaissance in the deployment of infrasound arrays will undoubtedly lead to large numbers of atmospheric exotic-source records in the near future (Bedard and Georges, 2000).

A common thread in exotic-source studies is quantification of the energy release of the source, at least in terms of magnitude and often in terms of spatial or temporal distribution as well. For sources such as bolides the motivation for investigation may be mainly based on scientific curiosity and the desire to document an unusual event; for cases such as mine collapses the motivation may include the testing of algorithms used to discriminate nuclear explosions from earthquakes. For incidents such as industrial accidents or terrorist attacks, however, investigation is additionally motivated by the potential utility of seismology and infrasound as forensic tools.

A specific exotic source that has recently been studied

*Present address: Saint Louis University, St. Louis, Missouri 63103.

forensically is vehicular bombings carried out by terrorists. Seismic records of at least two terrorist truck bombings are known to exist, and in both cases, the data were analyzed to estimate source properties (Holzer *et al.*, 1996; Koper *et al.*, 1999). The seismic data are valuable to investigators because they constrain the amount of energy released by the explosion (which can indirectly indicate the type of explosive used), the precise origin time of the explosion, and the number of discrete explosions that occurred.

We have obtained a unique data set for the study of vehicular explosions. The data consist of seismic (ground-motion) and acoustic (air-pressure) waveforms from a series of controlled truck bomb blasts carried out at White Sands Missile Range in New Mexico. We analyze these data to infer waveform properties that are well suited for yield estimation, to determine empirical functional relationships between explosive yield and the relevant waveform properties, and to compare the effectiveness of acoustic scaling laws with respect to seismic scaling laws. We demonstrate the forensic utility of the functional relations and scaling laws by applying them to seismic records of the 1998 truck bomb attack of the U.S. Embassy in Nairobi, Kenya (Crowe *et al.*, 1998).

The Dipole Might Test Series

The devastating 1996 terrorist attack on the Murrah Federal Building in Oklahoma City was recorded on a local seismograph and showed two pronounced wave trains. This led some to believe that multiple explosions had occurred and inflamed the antigovernment conspiracy theories of the time. Subsequent analysis of the seismic data showed that the two wave trains were an Earth structure effect that could easily be accounted for by a single source (Holzer *et al.*, 1996). Nevertheless, the controversy sparked by the initial uncertainty in the seismic analysis illuminated the need for a better understanding of the seismic properties of truck bomb explosions.

Owing to these and other facts, the Bureau of Alcohol, Tobacco, and Firearms (BATF) began sponsorship of a series of controlled vehicular explosions. The experiments, referred to as the Dipole Might (DM) test series, have been carried out by the Defense Threat Reduction Agency (DTRA) and the U.S. Army Engineer Research and Development Center at the White Sands Missile Range in New Mexico. The nominal intent of the DM program is to familiarize BATF agents with truck bomb debris patterns and to calibrate the effect of vehicular explosions on a variety of materials and structures.

The DM experiments have been heavily instrumented with diagnostic equipment including high-speed video cameras, which are used for studying fireball dynamics, time-of-arrival crystals, which are used to determine the velocity of the detonation front in the explosive material, and near-field (<50 m) pressure gauges, which are used to infer aspherical

properties of the atmospheric blast wave. Additionally, four of the DM explosions had pressure gauges and three-component short-period seismometers deployed at distances of 1–16 km (Fig. 1, Tables 1 and 2). Although the near-field gauges provide the most detailed source records, it is more important in a forensic sense to analyze the data recorded at local distances because it is at these ranges that data from actual terrorist attacks have been recorded.

The DM seismometers primarily record ground motion generated directly by the explosion but also record ground motion induced by the overpressure of the airblast as it propagates outward, as well as an extremely high-frequency signal associated with direct airblast-sensor interaction (Fig. 2). Detailed analyses of the coupling between acoustic overpressure and Rayleigh-wave propagation in the solid Earth has been presented by previous workers (Murphy, 1981; Murphy and Shah, 1988; Kitov *et al.*, 1997) and is not addressed here. The pressure gauges, in contrast, record energy that has traveled entirely through the air as a shock wave. Thus, acoustic waveforms differ considerably from seismic waveforms recorded at identical locations (Fig. 2).

The acoustic waveforms have sharper onsets, shorter durations, and fewer oscillations than the seismic waveforms, indicating that they represent nonelastic shock waves. Because dissipative effects are proportionally stronger in the ground than in the atmosphere, the airblast energy travels as a shock wave to much greater distances than the seismic

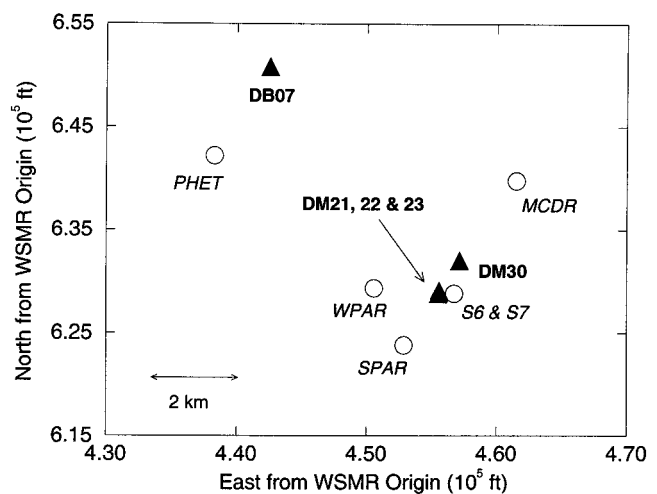


Figure 1. Source-receiver geometry for the four DM explosions discussed in the text. Each receiver location was occupied by a three-component short-period seismometer and a pressure gauge. Ground zero for tests DM21, DM22, and DM23 were almost identical, whereas ground zero for DM30 was slightly to the northeast. Receivers S6 and S7 were located adjacent to one another, however, S6 was deployed in an underground vault whereas S7 was deployed on the surface. The test area lies in the east-central part of the Jornada del Muerto, a deep alluvial valley in south-central New Mexico.

Table 1
Dipole Might Explosions

Test Name	Type of Explosive	Mass of Explosive (lb)	Atmospheric Pressure (mbar)	Atmospheric Temperature (K)	Number of Instruments
DM21	C4	10,000	844	280.8	4
DM22*	ANFO	20,000	850	293.0	1
DM23	C4	20,000	857	283.7	4
DM30	ANFO	10,000	855	284.8	7

*Shot time barometric information was unavailable for DM22, and so the listed value has been estimated.

Table 2
Airblast Properties

Explosion Name	Station Name	Distance (km)	Travel Time (sec)	Pulse Duration (sec)	Impulse (Pa sec)	Peak Overpressure (Pa)
DM21	WPAR	1.533	4.273	0.135	54.29	1105
DM21	SPAR	1.760	5.031	0.167	54.94	768
DM21	MCDR	3.804	10.92	0.145	25.16	338
DM21	PHET	6.654	19.30	0.212	6.86	186
DM22	MCDR	3.852	10.88	0.186	26.44	270
DM23	WPAR	1.530	4.285	0.182	92.71	1282
DM23	SPAR	1.794	5.094	0.187	89.61	1174
DM23	MCDR	3.770	10.82	0.198	42.15	428
DM23	PHET	6.630	19.45	0.246	24.54	325
DM30	S6	0.982	2.773	—	—	—
DM30	S7	0.983	2.773	0.135	82.15	1496
DM30	WPAR	2.169	6.253	0.155	35.44	513
DM30	MCDR	2.756	7.838	0.123	23.36	367
DM30	SPAR	2.807	8.164	0.130	26.35	393
DM30	PHET	6.548	19.19	0.187	11.41	119
DM30	S8	16.45	49.71	0.311	2.64	13

energy traveling in the solid Earth. For example, the hydrodynamic zone of a 1 kt nuclear explosion in granite has a radius of only about 5 m, and shock-induced fracturing ends at a radius of about 70 m; beyond this distance the energy travels through the Earth essentially elastically (Lamb *et al.*, 1991). Nevertheless, properties of both the elastic seismic waves and the nonelastic atmospheric waves can be used to estimate explosive yield and so are useful forensically.

The blast properties of the two explosives used in the DM experiments, ammonium nitrate fuel oil (ANFO) and C4, have been studied extensively. The former is commonly used by terrorists since it can be made from easily available materials. Sadwin and Pittman (1969) reported an explosive strength of approximately 80% (relative to trinitrotoluene [TNT]) for ANFO, and subsequent tests (General Electric Company–Tempo, 1977) support this value. Estimates of the explosive strength of C4 are more variable, in the range of 115%–160% (KG85), and in this study we use 130%. This percentage is consistent with the value given by Persson *et al.* (1994) and has been used previously in analyzing the seismic effects of C4 (Stump *et al.*, 1999). The nominal yields of the four well-instrumented DM shots become 3.6×10^3 kg TNT (DM30), 5.9×10^3 kg TNT (DM21), 7.3×10^3 kg TNT (DM22), and 12×10^3 kg TNT (DM23).

Data Analysis

Airblast Modeling

The pressure gauges deployed for the DM shots provided high-resolution records of the resulting atmospheric shock waves, which in turn contain large imprints of the source. An idealized shock wave (Fig. 3) can be completely described by three independent characteristics: (1) the initial shock intensity, which is manifested by the peak overpressure and by the travel time of the shock wave, (2) the positive phase pulse duration, and (3) the impulse per unit area of the blast wave, which is related to the decay of the pressure impulse. Each of these properties depends uniquely on the explosion type (chemical versus nuclear), the source-receiver distance, the atmospheric conditions, and the yield of the explosion.

One method of connecting observed shock characteristics with explosion source properties is through development of a hydrodynamic model describing the shock-wave evolution. However, the need for a sophisticated theoretical formulation can be circumvented by using dimensional analysis to derive general scaling laws among relevant model parameters. Once functional relationships have been calibrated for a controlled, reference explosion of known yield, the scaling

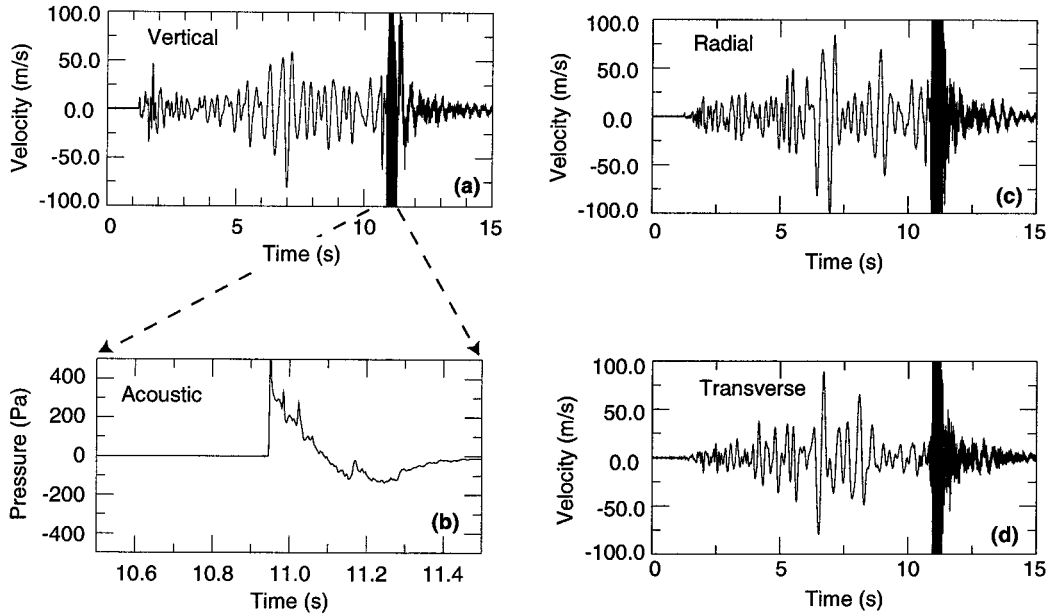


Figure 2. Seismic and acoustic records of the DM 21 truck bomb explosion carried out at White Sands Missile Range in New Mexico. The instruments were located 3.8 km northeast of ground zero at station MCDR. We show (a) vertical ground motion, (b) atmospheric overpressure, (c) radial ground motion, and (d) transverse ground motion induced by the detonation of 10,000 lb of C4. The seismic records primarily consist of elastic body and surface waves that have propagated through the Earth, while the acoustic record consists of the atmospheric shock wave. Note the difference in timescale between the acoustic and seismic records. Waveforms are clipped for purposes of illustration only.

laws can be used predictively on data observed from uncontrolled events of arbitrary size. Functional relations between airblast properties and model parameters have been documented for a reference chemical explosion of 1 kg TNT in air at 15°C (T_{ref}) and 1.01325 bars (P_{ref}) (Kinney and Graham, 1985; hereafter referred to as KG85).

Details on the development of airblast scaling laws are available from KG85 and Coppens and Reinhardt (1993) (hereafter CR93), and we only report the relations relevant to our analysis here. Scaling for source-receiver distance (r), peak overpressure (p_{peak}), average shock speed (σ), pulse duration (t_{dur}), and impulse per unit area (i_{area}) is given by

$$R = \left(\frac{f_d}{W^{1/3}} \right) r, \quad (1)$$

$$P_{\text{peak}} = \frac{(P_{\text{peak}})_{\text{obs}}}{P_{\text{obs}}}, \quad (2)$$

$$\Sigma \equiv \sigma_{\text{obs}} \frac{f_d}{f_t}, \quad (3)$$

$$T_{\text{dur}} = \left(\frac{f_t}{W^{1/3}} \right) t_{\text{dur}}, \quad (4)$$

$$I_{\text{area}} \equiv \frac{(i_{\text{area}})_{\text{obs}}}{f_d f_t W^{1/3}}, \quad (5)$$

where f_d and f_t are corrections for variation in atmospheric structure and are given by

$$f_d = \left(\frac{P_{\text{obs}}}{P_{\text{ref}}} \right)^{1/3} \left(\frac{t_{\text{obs}}}{T_{\text{ref}}} \right)^{-1/3}, \quad (6)$$

and

$$f_t = \left(\frac{P_{\text{obs}}}{P_{\text{ref}}} \right)^{1/3} \left(\frac{t_{\text{obs}}}{T_{\text{ref}}} \right)^{1/6}, \quad (7)$$

assuming the atmosphere behaves as an ideal gas. We adopt the notation of capital letters for scaled quantities and lowercase letters for observed quantities and define W as the ratio of the observed yield to the reference yield.

Equations (1)–(7) constitute the basis for relating airblast properties of observed explosions to airblast properties of the reference explosion. Since the functional dependencies (relationships between R and P_{peak} , Σ , I_{area} , and T_{dur}) have been determined for the reference explosion, it is possible to estimate the yield of observed explosions with respect to the reference yield. It is important to note, however, that the reference data were obtained for an idealized, spherical ex-

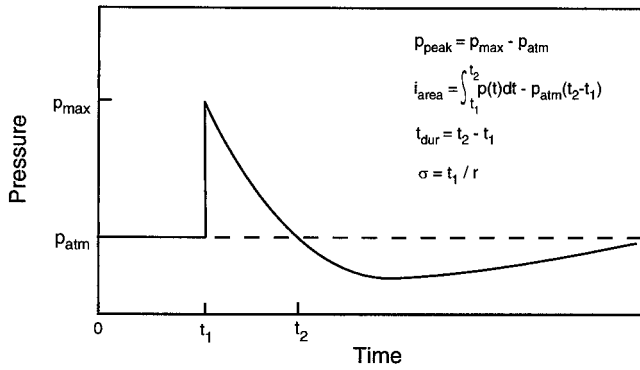


Figure 3. Idealized model used for interpretation of the airblast data. The initial pressure discontinuity and subsequent quasi-exponential decay distinguish the airblast as a shock wave rather than an elastic wave. We investigate the utility of four airblast properties, p_{peak} , i_{area} , t_{dur} , and σ , as indicators of explosive yield using the DM data set.

plosive charge, and so the functional relations of actual chemical explosions, such as truck bombs, may differ significantly from what is predicted.

In the following sections we investigate how well the reference functional relations describe the DM data. Since the yields of the DM shots are known we develop independent functional relations that are specific to the DM truck bomb data. We also examine the relative quality of the airblast properties as yield estimators for the scaled distance range that is appropriate to truck bomb explosions.

Peak Overpressure. A typical pressure gauge recording of a DM shot is highlighted in Figure 4a. The instrument response of the modified Validyne differential pressure gauges used for the DM experiments (Reinke, 1985) is essentially flat between 0.05 and 200 Hz; however, the finite response time of the gauges causes the observed overpressure-time history to differ from that of the idealized shock wave presented in Figure 2. In general, the nominal peak overpressure underestimates the true value. To obtain accurate observations of peak overpressure, p_{peak} , we follow the procedure suggested in KG85 and fit a line to the logarithm of the overpressure-time curve, neglecting the first few points of the record that constitute the initial upswing of the shock wave. We use the antilog of the intercept of this line as the p_{peak} observation. An example log-linear fit is presented in Figure 4b.

This procedure introduces a measure of subjectivity in choosing the points to include in the log-linear fit, however, the variability is small compared to the gain in accuracy of the p_{peak} estimate. We find that using the log-linear extrapolation increases the correlation of p_{peak} observations with distance and yield relative to using the nominal values. The p_{peak} observations for each source-receiver combination in the DM series are listed in Table 2 and illustrated in Figure 5a. The clear separation of the data by shot number supports

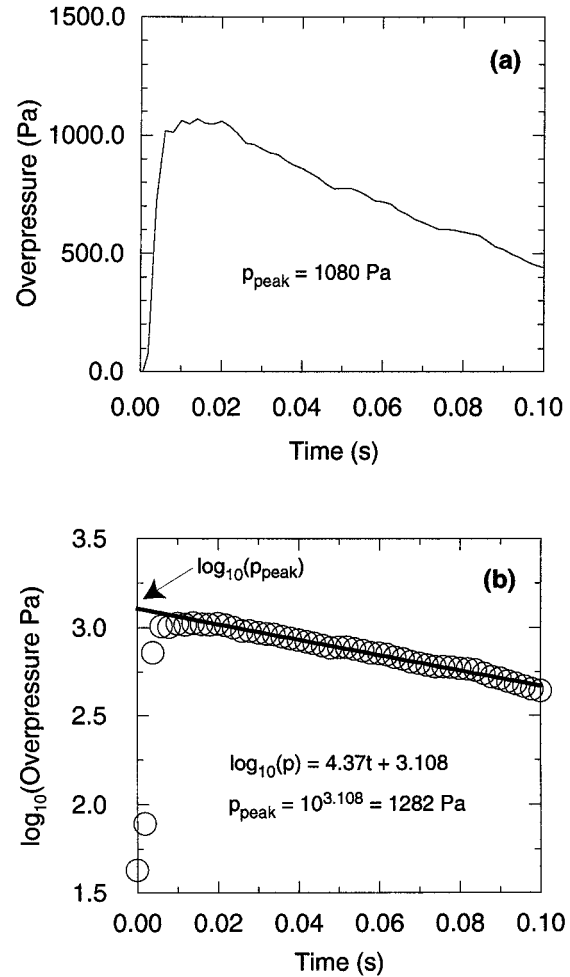


Figure 4. Close-up of the airblast arrival for the station 1.53 km to the west of the DM23 shot (WPAR). We show the data in (a) linear-linear space and (b) \log_{10} -linear space. Owing to the response of the pressure gauge the shock wave has a finite rise time that must be accounted for when estimating the peak overpressure, p_{peak} . We extrapolate a linear fit to a subset of the data in \log_{10} -linear space to estimate p_{peak} . Use of this procedure increases the measurement accuracy.

the idea that p_{peak} values are relevant for yield estimation in the range of scaled distances sampled by the DM shots.

The dependence of p_{peak} on r for the reference chemical explosion is described in terms of the corresponding scaled variables as (KG85)

$$P_{\text{peak}}(R) = \frac{808 \left(1 + \left(\frac{R}{4.5}\right)^2\right)}{\left[\left(1 + \left(\frac{R}{0.048}\right)^2\right)\left(1 + \left(\frac{R}{0.32}\right)^2\right)\left(1 + \left(\frac{R}{1.35}\right)^2\right)\right]^{1/2}}, \quad (8)$$

where P_{peak} is dimensionless and R is in m. As R becomes large the shock wave decays into an elastic wave that has energy proportional to R^{-2} ; since the energy in an elastic

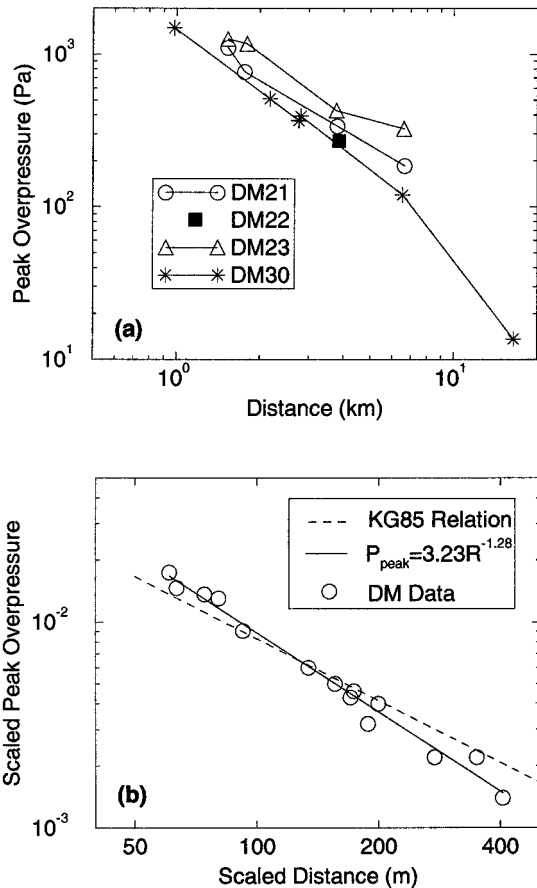


Figure 5. The peak overpressure observations from the DM airblasts shown in (a) raw form and (b) scaled form. The raw data are clearly separated according to explosion, confirming the utility of p_{peak} as a yield estimator. The standard reference relation between scaled distance, R , and scaled peak overpressure, P_{peak} , fits the DM data well, although we determine a slightly more accurate relation that is specific to the DM data. The datum from the most distant station for DM30 is not included in the calculation because at this range the airblast has decayed into an elastic wave.

wave is also proportional to the square of the pressure, P_{peak} becomes proportional to R^{-1} .

Given an (r, p_{peak}) observation and measurements of the ambient pressure and temperature, we combine equations (1), (2), (6) and (7) with equation (8) to define an implicit function of the yield ratio, W . We solve this function numerically to generate a single station estimate of W . As an example DM21 generated a p_{peak} value of 1105 Pa, at a distance of 1530 m, with the local weather such that $p_{\text{obs}} = 844$ mbar and $t_{\text{obs}} = 8^\circ\text{C}$; plugging these values into the appropriate equations, we find that the yield ratio, W , is 1.2×10^4 . Since the reference explosion relation is calculated for a yield of 1 kg TNT, this single station yield estimate for DM21 becomes 1.2×10^4 kg TNT.

The robustness of p_{peak} yield estimates can be increased

when more than one pressure record of the same explosion are available. For instance, in the case of DM21 the three additional single station yield estimates are 6.1×10^3 kg TNT, 5.3×10^3 kg TNT, and 4.7×10^3 kg TNT. Taking the \log_{10} average of the four single-station estimates gives a yield of 6.5×10^3 kg TNT, which is in good agreement with the actual DM21 yield of 5.9×10^3 kg TNT.

Alternatively, we can find the yield ratio, W , which provides the best simultaneous fit to all the (r, p_{peak}) data points. Using a one-dimensional search of W values, we minimize the root mean square error of the difference between the observed and predicted p_{peak} values. We compute the error in \log_{10} space so that the yield estimate is not overly biased by the nearest receivers. In this case the DM21 yield estimate, 6.6×10^3 kg TNT, is not significantly different from the previous value (6.5×10^3 kg TNT).

We generate standard errors for the multistation yield estimate using a bootstrap technique. We assign uncertainties of 5.0 m for each r value and approximately 10 Pa for each p_{peak} value. We then define a series of Gaussian distributions for both r and p_{peak} that have as means the observed data values and as standard deviations the designated uncertainties. We randomly select values from these distributions to create a series of N artificial data sets of (r, p_{peak}) values. For each of these artificial sets we find the best-fitting value of W using the multistation technique described previously. We then use the standard deviation of the N values of W as a proxy for the standard error of the actual optimal W value. We find that the standard error tends to converge for $500 < N < 1000$. As defined, these standard error estimates account only for observational uncertainties and do not account for systematic sources of error such as inaccuracies in the functional R - P_{peak} relationship.

We report optimal multistation yield estimates and the corresponding standard errors for each of the DM shots in Table 3. For the DM30 fit, we neglect using data from the furthest station because at this range the airblast has become elastic and so its amplitude is much less robust than the others. In general the yield estimates are well correlated with the actual yields and within one standard deviation of the actual yields. The exception is DM22, which gives an abnormally small value. This shot, however, was recorded by only a single instrument and so is more poorly constrained than the others. In general, our results indicate that p_{peak} observations have value as yield estimators for the scaled distance range where truck bomb explosions are likely to be observed.

The results in Table 3 also imply that the reference chemical explosion relation (equation 8) provides a good description of the evolution of p_{peak} with distance for truck bomb explosions. We quantify this by comparing its predictions with the actual scaled data from the DM shots (Fig. 5b). The reference predictions differ only slightly from a least-squares regression of the data. This is consistent with the high accuracy of the p_{peak} yield estimates. Nevertheless, our empirical relation,

Table 3
Acoustic Yield Estimates from Reference Relations*

Test Name	Actual Yield	p_{peak} Yield	i_{area} Yield	t_{dur} Yield	σ Yield
DM30	3.6	3.0 ± 1.5	7.9 ± 0.3	36.0 ± 1.4	4.3 ± 1.7
DM21	5.9	6.6 ± 2.9	8.5 ± 0.5	51.0 ± 1.9	24.2 ± 4.0
DM22	7.3	2.7 ± 2.9	13.0 ± 0.8	73.0 ± 4.9	67.8 ± 12.0
DM23	12.0	17.0 ± 4.7	23.0 ± 0.5	98.0 ± 3.0	18.3 ± 3.2

*Units of 10^3 kg TNT.

$$P_{\text{peak}} = 3.32R^{-1.28} \text{ for } 50 < R < 400, \quad (9)$$

does give a slightly better description of the DM data and is in a simpler form than the standard reference relation.

Blast Wave Impulses. The impulse per unit area (i_{area}) of a shock wave may be the most reliable indicator of explosive yield since momentum is conserved as the shock front interacts with the pressure gauge. We calculate i_{area} for each airblast record by integrating from the shock onset to the beginning of the negative rarefaction phase. The i_{area} values are listed in Table 2 and illustrated in Figure 6a. Similar to the p_{peak} observations the i_{area} curves for the various DM shots are clearly separated, indicating that i_{area} is likely to be a good yield estimator.

The relation between i_{area} and r in terms of corresponding scaled variables is given as (KG85):

$$I_{\text{area}}(R) = \frac{0.067 \left(1 + \left(\frac{R}{0.23} \right)^4 \right)^{1/2}}{R^2 \left(1 + \left(\frac{R}{1.55} \right)^3 \right)^{1/3}}, \quad (10)$$

or alternatively (CR93),

$$I_{\text{area}}(R) = \frac{1.05}{\left(1 + \left(\frac{R}{1.5} \right)^{10} \right)^{1/10}}, \quad (11)$$

where I_{area} has units of mbars, and R is in m. Given an (r , i_{area}) observation we combine equations (1), (5), (6), and (7) with either equation (10) or (11) to define an implicit function of W . Analogous to the p_{peak} procedure, this function can be solved numerically for a single station estimate of W or combined with other (r , i_{area}) observations in a simultaneous fit. We follow the latter approach and estimate the standard errors using the previously described bootstrap procedure with uncertainties of 5.0 m for r and 1.0 Pa sec for i_{area} . The results using equation (10) are reported in Table 3.

The corresponding yield estimates are significantly higher than the theoretical values. Using equation (11) in lieu of (10) in the estimation process gives even higher yield estimates; however, in both cases the yield estimates correlate well with the actual yields. This is true even for DM22 in which only a single i_{area} value was available. This corre-

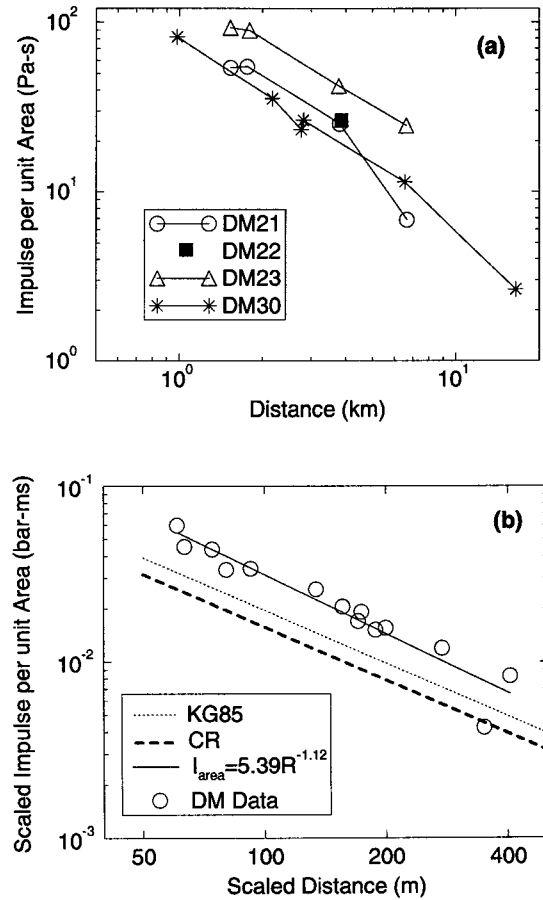


Figure 6. The impulse per unit area observations from the DM airblasts shown in (a) raw form and (b) scaled form. The raw curves are clearly separated according to yield, although the most-distant DM21 observation appears anomalous. The scaled data are highly correlated, adding support to impulse per unit area as a yield indicator, but are poorly described by two pre-existing standard functional relations. The functional relation defined by a least-squares linear regression of the scaled data is a much more accurate description of the DM data. We again omit the most distant DM30 datum since the airblast is elastic at this range.

lation supports the idea suggested by Figure 6a that i_{area} observations are useful for yield estimation but implies that the standard reference relations (equations 10 and 11) do a poor job of describing the DM observations.

We confirm the fundamental utility of i_{area} observations for yield estimation by showing the correlation between R and I_{area} for the DM data (Fig. 6b). We perform a linear regression on these data to define the following functional relation that provides an accurate description of the dependence of I_{area} on R for the DM data:

$$I_{\text{area}} = 5.39R^{-1.12} \text{ for } 50 < R < 400. \quad (12)$$

Pulse Duration. A third airblast property that may have utility as a yield estimator is the pulse duration, t_{dur} . We define t_{dur} as the time between the shock onset and the end of the initial positive phase pulse. Observations of t_{dur} for each of the DM records are listed in Table 2 and illustrated in Figure 7a. The t_{dur} curves for each shot separate somewhat but there is more scatter than with the raw p_{peak} and i_{area} data. This is partially related to the fact that t_{dur} varies by a factor of only 2–3 over the DM scaled distance range, while p_{peak} and i_{area} vary by orders of magnitude.

The following expression relating t_{dur} and r in terms of the scaled variables is available from KG85,

$$T_{\text{dur}}(R) = \frac{980 \left(1 + \left(\frac{R}{0.54} \right)^{10} \right)}{\left(1 + \left(\frac{R}{0.02} \right)^3 \right) \left(1 + \left(\frac{R}{0.74} \right)^6 \right) \left(1 + \left(\frac{R}{6.9} \right)^2 \right)^{1/2}}, \quad (13)$$

where T_{dur} has units of msec and R is in m. Combining equations (1), (4), (6) and (7) with equation (13) we again have an implicit function of the yield ratio W .

We perform a multistation fit for each DM shot, this time computing the error in regular (non- \log_{10}) space. The standard errors for each yield estimate are calculated with the bootstrap technique using uncertainties of 5.0 m in r and 4.0 msec in t_{dur} . The results from these calculation are reported in Table 3.

These t_{dur} yield estimates are all substantially higher than the theoretical yields by a factor of ~ 10 ; however, similar to the i_{area} estimates the t_{dur} yields are well correlated with the theoretical yields. This suggests that t_{dur} is a useful yield estimator for the our scaled distance range, but that the reference chemical explosion relation does a poor job of describing the DM data.

We illustrate the (R, T_{dur}) points for all the DM data in Figure 7b. The reference relation, equation (13), is included for comparison and is seen to provide a gross underestimate of the data. It follows that yield estimates based on t_{dur} observations will be substantially high if the reference relation is used. The following empirical relation, obtained from a least squares regression, provides a better fit to the truck bomb data:

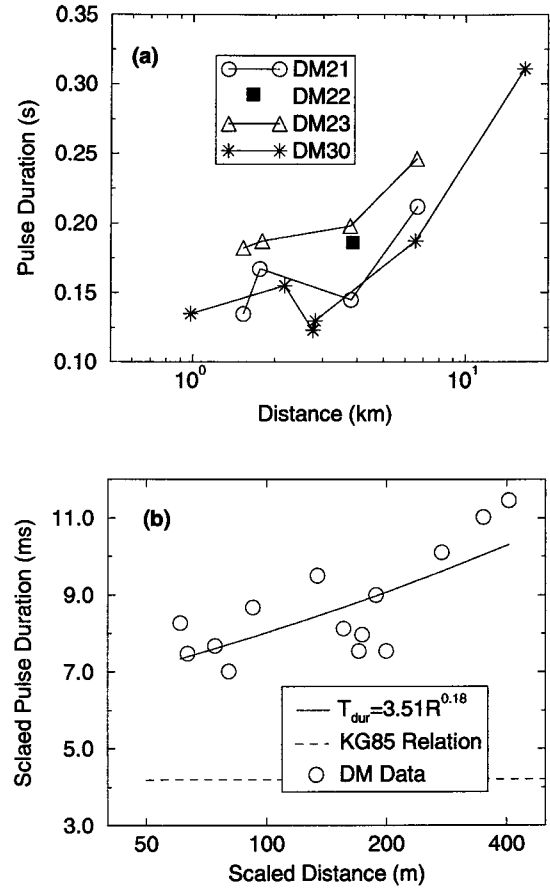


Figure 7. The positive phase pulse duration from the DM airblasts shown as (a) raw data and (b) scaled data. The separation of the raw data curves according to yield corroborates the usefulness of the pulse duration as a yield indicator. However, the pulse duration changes magnitude only by a factor of 2 over the distance range, whereas p_{peak} and i_{area} vary by several orders of magnitude (Figs. 5 and 6). Thus observational uncertainties induce a proportionally larger scatter in the scaled data. Nevertheless, the variation is large enough that t_{dur} is a viable yield estimator, though the pre-existing reference relation describes the DM data poorly.

$$T_{\text{dur}} = 3.51R^{0.18} \text{ for } 50 < R < 400, \quad (14)$$

where T_{dur} is in msec and R is in m.

Airblast Travel Times. The final airblast property we examine for use as a yield indicator is the shock-wave travel time, tt . In contrast to an elastic wave, the velocity at which a shock wave travels is a function of the source magnitude as well as the elastic structure of the medium through which it propagates. As the shock waves loses energy and decays into an elastic wave, its velocity slows and approaches the elastic wavespeed. The shock-wave travel time is the only airblast property that can be determined with seismic data alone. This is possible because an airblast often produces an

easily observable, impulsive, high-frequency arrival when directly interacting with seismometers (Fig. 2).

It is common to consider the average shock velocity, $\sigma = r/tt$, instead of the shock-wave travel time (tt) itself. This provides little difficulty from our perspective of yield estimation because r is likely to be precisely determined whether an explosion is planned or not. For uncontrolled explosions it may be difficult to obtain the precise origin time, however, this uncertainty affects yield estimation based on tt in the same manner as yield estimation based on σ . We note that of the four airblast yield indicators it is only σ that is sensitive to uncertainties in absolute time.

We illustrate the σ observations for the DM data in Figure 8a and list the values in Table 2. The curves specific to each explosion separate somewhat, but less so than for the three other airblast properties (Figs. 5a, 6a, and 7a); however, the trend of σ decreasing with increasing distance is clear. The raw DM22 datum is particularly anomalous partially owing to the relatively high temperature at shot time (cf. Table 1).

The dependence of σ on r for the reference chemical explosion is given in terms of the scaled variables as (CR93):

$$\Sigma(R) = \frac{1960}{R^{9/10}} \left(1 + \left(\frac{R}{5.2} \right)^{14/5} \right)^{2/7} \left(1 + \left(\frac{R}{70} \right)^2 \right)^{1/20}, \quad (15)$$

where Σ has units of m/sec as and R has units of m. Combining equations (1), (3), (6), and (7) with (15) we generate implicit functions of W . We compute multistation yield estimates and standard errors using the procedures described earlier and list the results in Table 3. We use uncertainties of 5.0 m in r and 4.0 msec in tt .

The estimated yields for DM23 and DM30 agree well with the theoretical yields and have an appropriate ratio, but the DM21 and DM22 yields are substantially high. We are unable to determine a unique explanation for the DM22 yield, but it is likely that atmospheric conditions that are unaccounted for, such as a wind gust, are to blame. In the case of DM21 we feel that increased atmospheric water content is responsible. The relative humidity at the time of DM21 shot was 95% (DeRego, 1997) and, indeed, a thick blanket of fog covered the area. It is well known that wave-speed in air increases with humidity, however, the atmospheric transmission factors f_d and f_t only compensate for pressure and temperature variations. Thus it is likely that for DM21 the ambient atmospheric wavespeed was significantly greater than normal because of the humidity and that since this effect was unaccounted for in the scaling relation (equations 6 and 7), the DM21 yield estimate is anomalously high.

We show Σ for all the DM data in Figure 8b. However we make a point of distinguishing DM21 and DM22 data from DM23 and DM30 data. The latter data group is well modeled by the standard relation, as expected from the accurate yield estimates, whereas the former data values are greater than the predictions. We define an alternative scaling

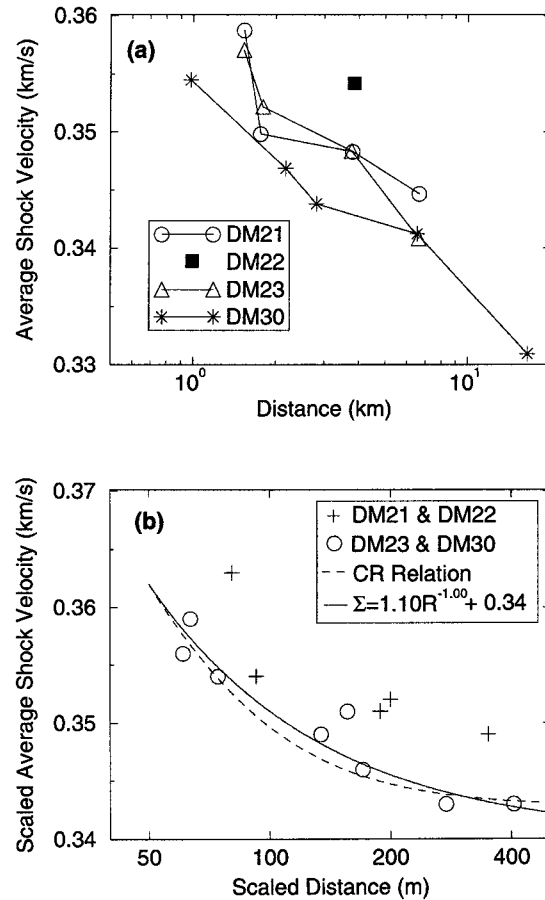


Figure 8. The average shock velocity of the DM airblasts presented as (a) raw data and (b) scaled data. The DM22 datum is anomalous partly because of the relatively high shot-time temperature. Explosions DM23 and DM30 separate from each other in the raw data, but the DM21 curve appears anomalously fast. We attribute this to increased ambient wavespeed induced by a heavy fog at the time of DM21 shot. The trend in scaled velocities for DM23 and DM30 is well fit by the reference standard relation, and a linear regression gives only modest improvement.

relation by regressing only the data from DM23 and DM30 (Σ in m/sec and R in m):

$$\Sigma = 1100R^{-1.00} + 340 \text{ for } 50 < R < 400, \quad (16)$$

however, it provides only a modest improvement from the standard reference relation.

Seismic Analysis

The seismic waveforms from the DM explosions are more complicated than the acoustic waveforms (cf. Fig. 2) because shallow geologic structure is substantially more complex than near-surface atmospheric structure. Over the distance scale relevant to the DM explosions the atmosphere is well (though not completely) described by only two easily observable parameters, p_{obs} and t_{obs} . The relevant geologic structure, on the other hand, is dependent on a larger number

of less accessible parameters. The primary consequence of this fact is that the seismic scaling laws will be based on a truncated set of model parameters and so be less portable than the acoustic scaling laws. Furthermore, variations in along-path anelastic (Q) structure, which can depend on subtle features such as water table depth, can indirectly degrade the accuracy of seismic scaling laws.

A review of previous work on scaling relations between seismic observables and yield is given in Denny and Johnson (1991). Here we assume that the Earth structure can be defined by two parameters, density and velocity, and look for empirical relations between yield and a series of seismic observables related to the seismic source function. The observables are the peak displacement of the P wave, a proxy of the seismic moment, the corner frequency, and the decay rate of the high-frequency part of the spectrum.

The near-source region for a DM shot typically consists of a thin layer of concrete (thickness of 25 cm, density of 2.8 g/cm^3), overlaying a thicker layer of compacted soil (thickness of 50 cm, density of 2.1 g/cm^3), overlaying the ambient soil (density of ~ 1.6 to a depth of 5 m) (DeRego, 1997). Refraction surveys and borehole sampling of the DM region show unconsolidated alluvium with a P -wave velocity of $\sim 1 \text{ km/sec}$ down to the water table depth of 70–80 m (Reinke, 1981). It is unclear how large a role the thin layer of concrete plays, but it is probable that the *in situ* material below is most important, and we designate the effective source density to be 1.6 g/cm^3 and the effective source P -wave velocity to be 1.0 km/sec .

Peak Displacement of First Arrival. The time domain amplitude of the first-arriving P wave is often used in defining the magnitude of a seismic event. It has value as a yield estimator since the radiation patterns of explosions tend to be simpler and more isotropic than those of earthquakes. Furthermore, the P -wave amplitude is less influenced by scattered energy than later-arriving phases, and so the portability of scaling laws based on P -wave amplitude should be enhanced.

The initial polarity on the vertical and radial components of ground motion is compressive for all of the DM records, consistent with the explosive nature of the truck bomb sources. We estimate the peak P -wave displacement, μ_{peak} for each source-receiver combination using the following procedure. We remove the mean and trend from each seismogram, integrate from velocity to displacement, and apply a bandpass filter from 0.5 to 5.0 Hz. We compute μ_{radial} and μ_{vertical} by subtracting the displacement at the arrival time of the phase from the displacement at the first peak. We then define μ_{peak} as

$$\mu_{\text{peak}} = \sqrt{\mu_{\text{radial}}^2 + \mu_{\text{vertical}}^2} \quad (17)$$

so that the angle of incidence of the ray does not bias the yield estimate. We illustrate the μ_{peak} measurements for the DM data in Figure 9a.

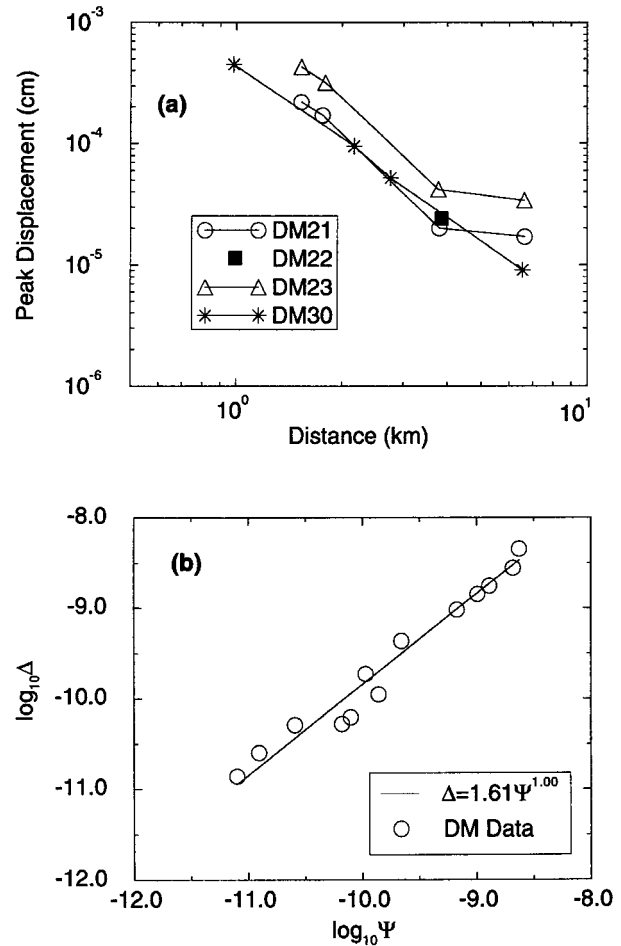


Figure 9. The peak displacement, μ_{peak} , of the initial seismic pulse for each of the DM records as (a) raw data and (b) the corresponding dimensionless parameters. Definitions for Δ and Ψ are given in the text. The separation of the raw data according to yield and the high correlation of the dimensionless parameters signify that μ_{peak} is relevant for yield estimation. The functional relation we derive between Δ and Ψ is applicable to seismic yield estimation of chemical explosions, though it is not as portable as the airblast relations.

We use dimensional analysis to determine an appropriate form for the μ_{peak} scaling law. We define the relevant model parameters as explosive mass m , distance r , density ρ , and compressional wavespeed α , and we assume that μ_{peak} is some power-law function of the model parameters. Balancing the units gives the following relationship,

$$\Delta = k_{\Delta} \times \Psi^{A_{\Delta}}, \quad (18)$$

where the dimensionless, or scaled, variables are defined as

$$\Delta \equiv \frac{\mu_{\text{peak}}}{r}, \quad \Psi \equiv \frac{m}{\rho r^3}, \quad (19)$$

and k_{Δ} and A_{Δ} are the constants to be determined.

We present the relation between Δ and Ψ for the DM data in Figure 9b. The two variables are extremely well correlated in \log_{10} space with a coefficient above 0.98. This correlation is artificially increased to a certain degree, since both dimensionless variables depend on r ; However the correlation between raw μ_{peak} values and Ψ remains high with a coefficient of 0.97. A least-squares regression gives the following functional relationship:

$$\Delta = 1.61\Psi^{1.00} \text{ for } 10^{-11} < \Psi < 10^{-8.5}. \quad (20)$$

The standard errors for k_{Δ} and A_{Δ} are listed in Table 4. The following simple corollary relating the unscaled variables results from substituting equation (19) into (20):

$$m \approx \mu_{\text{peak}} r^2, \quad (21)$$

where m is in g and μ_{peak} and r are in cm.

We examine the sensitivity of the μ_{peak} scaling laws to the type of explosive by doing separate regressions for the DM data generated by C4 and ANFO (Table 4). The A_{Δ} values are not significantly different, and so a single scaling law is valid, provided the explosive masses are scaled correctly. We check the relative explosive strength of ANFO and C4 by doing linear regressions with the slope (A_{Δ}) fixed at 1.0 and find the ratio of k_{Δ} values to be 0.45. This value is smaller than the 0.61 ratio we have assumed in generating the overall fit (equation 20), but considering the standard error, it is not appreciably different.

Low-Frequency Asymptote of Displacement Spectra. A second property of seismic waveforms that is expected to have a strong dependence on yield is the low-frequency asymptote of the displacement spectrum, Ω_0 . This quantity is often used to compute the scalar seismic moment, M_0 , in source studies. For instance, a commonly used relation is given as

$$M_0 = 4\pi r c^2 \Omega_0, \quad (22)$$

where c is either the compressional or shear velocity, depending on which component of ground motion is analyzed (i.e., Stump and Reinke, 1991).

We calculate Fourier transforms of the displacement seismograms for time windows that start about 1 sec before the first arrival and end after the airblast arrival has decayed below the noise level. Furthermore, each time series is padded with zeros until the number of points is a power of 2. We compute the amplitude at a specific frequency by mul-

tiplying the modulus of the complex transformed variable by the sampling interval in the time domain, resulting in units of m sec.

The amplitude spectra are unaffected by small changes in the definition of the time window and are generally flat for frequencies of approximately 1–5 Hz with sharp decreases on either side of the flat region. The spectral fall-off at low frequencies is due to instrumental limitations, and it is the height, or offset, of the flat portion of the spectra that we refer to as the low-frequency asymptote. We model the spectra in the range of approximately 0.5–10 Hz using a simple three-parameter template: the intercept of the flat portion, the corner frequency, and the decay rate (slope) for the high frequencies. For each spectrum we do a series of increasingly fine grid searches to find the parameters that minimize the root mean square error between the model and data. A typical DM spectrum, along with the best-fitting model, is presented in Figure 10.

The low-frequency asymptotes for the radial and vertical components show a clear decrease with distance. We show their average for all of the DM data in Figure 11a. Similar to the μ_{peak} data shown in Figure 9a, the Ω_0 curves separate according to shot number. The separation is not as clear as for some of the airblast properties, but it nevertheless implies that Ω_0 can be an effective yield estimator in this scaled distance regime.

The spectra of the transverse components show a more complicated behavior. The transverse energy arises mainly from scattering since the DM sources are too small for spall or tectonic release to play a role. The DM data are well described by the model of Gupta and Blandford (1983) in which the ratio of SV/SH from explosions is high at small distances and approaches unity at larger distances as scatterers are progressively encountered. We find ratios of radial

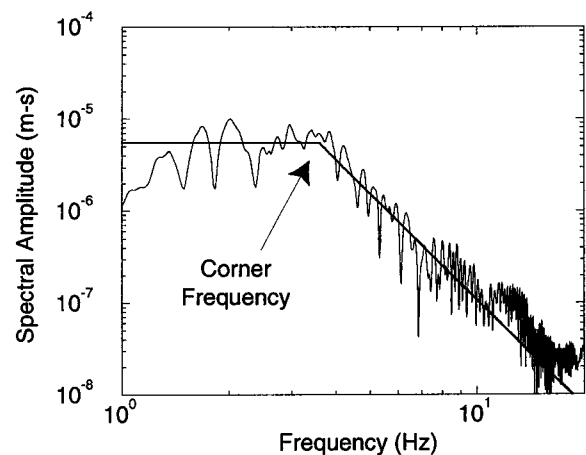


Figure 10. Displacement amplitude spectrum from the radial component of motion recorded by the station 2.17 km to the west of DM30 (WPAR). The best-fitting spectral model is shown as well. We use the offset of the flat portion of the spectrum, Ω_0 , as a yield estimator.

Table 4
Dimensionless Seismic Functional Relations

Data Set	A_{Δ}	$\log_{10}(k_{\Delta})$	A_{Γ}	$\log_{10}(k_{\Gamma})$
All	1.00 ± 0.05	0.21 ± 0.51	1.13 ± 0.08	2.01 ± 0.79
ANFO	1.05 ± 0.08	0.63 ± 0.74	1.16 ± 0.11	2.36 ± 1.02
C4	0.96 ± 0.07	-0.12 ± 0.72	1.12 ± 0.07	1.91 ± 0.65

Ω_0 to transverse Ω_0 that smoothly decay from 4–5 to 1 as distance increases. Owing to this behavior we use the average Ω_0 from the radial and vertical components and omit the transverse component in defining the dimensionless functional relation.

We assume as before that the seismic observable, Ω_0 , is a power-law function of explosive mass m , distance r , density ρ , and compressional wavespeed α . Balancing the units we define the following dimensionless variable,

$$\Gamma \equiv \frac{\Omega_0 \alpha}{r^2}, \tag{23}$$

which is related to the normalized yield (Ψ) defined in equation (19), by a specific power law:

$$\Gamma = k_\Gamma \times \Psi^{A_\Gamma}, \tag{24}$$

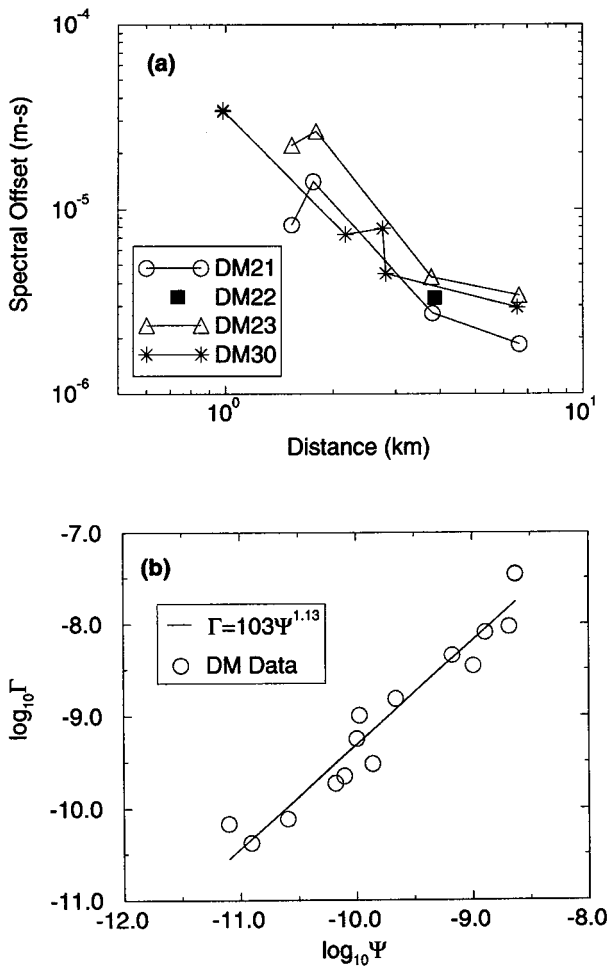


Figure 11. The average of radial and vertical spectral offsets for each DM source-receiver combination as (a) raw data and (b) corresponding dimensionless parameters. Definitions of Γ and Ψ are given in the text. The separation of the raw data curves with yield is not as clear as in the previous case (Fig. 9); however, the offset values still contribute to yield estimation.

where k_Γ and A_Γ are again constants to be determined.

We present the relation between Γ and Ψ for the DM data in Figure 11b. The results of a least-squares linear regression in \log_{10} space are presented in Table 4. The variables are highly correlated with a coefficient of 0.97. This value is biased toward the high end because Γ and Ψ mutually depend on r , but the bias is small as the correlation coefficient of the unscaled Ω_0 values and Ψ values is 0.93.

We separate the (Γ , Ψ) data into two subsets according to whether the shots consisted of C4 or ANFO. The results of least-square linear regressions on these subsets are listed in Table 4. Analogous to the (Δ , Ψ) data the exponents do not differ significantly between types of explosive. We regress each subset with a constant slope of 1.15 and find the ratio of k_Γ for ANFO to C4 to be 1.04. The error associated with this ratio overlaps our assumed ratio of 0.61; however, it is much less closer than the μ_{peak} ratio of ANFO to C4. This favors μ_{peak} as a more precise yield estimator than Ω_0 .

Corner Frequencies and Decay Rates. We next examine the corner frequencies from DM spectra as potential yield estimators. It is well known in earthquake seismology that corner frequency decreases as earthquake size increases, and corner frequencies have often been considered in scaling studies of explosion spectra as well (Denny and Johnson, 1991). The best-fitting corner frequencies from the spectral grid searches are illustrated in Figure 12. The frequencies are all in the range of 2–5 Hz but the curves do not separate by shot. This is the case for both the radial and vertical components. The frequency values are also uncorrelated with normalized yield, Ψ , and so we conclude that corner frequencies are not relevant to yield estimation over the distance-yield combinations sampled by the DM experiments. The decay rate of the high frequencies, or rolloff, is normally assumed to be constant for a given source model

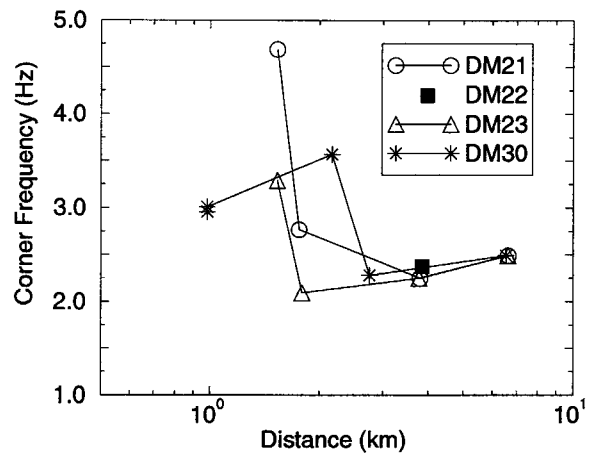


Figure 12. Corner frequencies of the radial displacement spectra for all of the DM data. The data are not well separated by shot number, and so for these yield-distance combinations corner frequency cannot be used to estimate the yield.

and so is not particularly useful for yield estimation. We show the rolloffs obtained for the DM data in Figure 13. As expected there is no clear trend, and the observations tend to support a seismic source model with a rolloff of -3 .

Applications of the Dipole Moment Scaling Laws

We have access to data from two chemical explosions that provide the means for a partial evaluation of the DM scaling laws. The first data set are seismic and acoustic waveforms of a surface chemical explosion carried out at White Sands Missile Range. The explosion was substantially smaller than the DM shots, and it was not contained within a vehicle; however, the geologic structure of the region is similar to that of the DM shots.

The second data set consists of a three-component, broadband seismic record of the Nairobi, Kenya, truck bomb blast of 7 August 1998. In this case the source geometry is well mimicked by the DM shots, but the geologic structure may be significantly different than that at White Sands. Hence, these two explosions are complementary in testing and illustrating the DM derived functional relations.

The Divine Buffalo Experiment. A controlled explosion of 1000 lb of C4 was recently carried out at White Sands Missile Range with the code name Divine Buffalo 7 (DB07). The charge was detonated on a thin wooden platform about 1 m off the ground, and about 3 m from a four-story building. The nominal intent of the DB07 experiment was to test the response of building materials to an explosive blast, however, we were able to deploy seismic and acoustic instruments at local distances. At shot time the barometric pressure was 848.6 mbar and the temperature was about 11.5°C .

For the DB07 shot we deployed three-component, short-period seismometers at four sites: two were adjacent to one another 8.0 km southeast of ground zero (S1A above ground, and S1B buried), a third was located 2.9 km to the southwest (S2), and the fourth was placed 1.0 km to the west (S3). A pressure gauge was also deployed at S1A, and the electric potential between two rods located 50 m and 200 m north of ground zero was recorded as well, providing an extremely precise measurement of the origin time.

The DB07 airblast properties recorded by the pressure gauge at S1A ($R \sim 900$ m) are listed in Table 5. The large scaled distance implies that the airblast has become nearly elastic, and so its properties may be less sensitive to the source characteristics than the DM data. Also, the DM functional relations were defined for $50 < R < 400$ m, and extrapolation to larger distances causes increased uncertainty.

We perform single-station yield estimates for S1A based on p_{peak} , t_{dur} , and i_{area} observations. In each case we use the functional relationship between scaled variables determined from the DM data. We calculate the standard errors using the previously described bootstrap technique assuming uncertainties of 5.0 m in r , 10.0 Pa in p_{peak} , 4.0 msec in t_{dur} , and 0.5 Pa sec for i_{area} . The results are reported in Table 5.

The i_{area} -based estimate is the most accurate and is

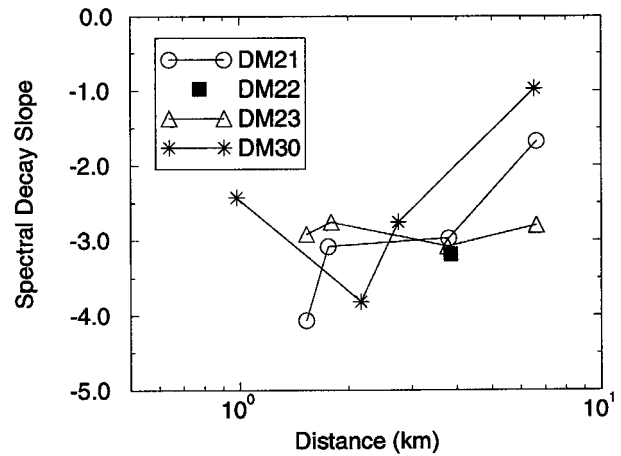


Figure 13. The rolloff, or decay rate, of the high-frequency spectral amplitudes. The observations are not relevant to yield estimation however we present them for completeness. The values support a source model with a rolloff of -3 for the truck bomb explosions.

Table 5
Divine Buffalo 7 Yields from DM Relations

Yield Type	Yield Value (10^3 kg TNT)	Stations Used	Data Used
Actual	0.59	—	—
i_{area}	0.74 ± 0.23	S1A	2.03 (Pa sec)
t_{dur}	0.39 ± 0.06	S1A	0.095 (s)
p_{peak}	5.35 ± 4.76	S1A	121.4 (Pa)
σ	20.3 ± 5.73	S1A	342 (m/sec)
σ	12.1 ± 4.06	S1B	341 (m/sec)
σ	2.90 ± 2.37	S2	344 (m/sec)
σ	0.59 ± 0.61	S3	347 (m/sec)
σ	0.83 ± 0.73	all	—
μ_{peak}	0.82 ± 0.33	S1A	1.3×10^{-8} (m)
μ_{peak}	0.63 ± 0.31	S1B	1.0×10^{-8} (m)
μ_{peak}	0.47 ± 0.04	S2	5.6×10^{-8} (m)
μ_{peak}	0.78 ± 0.01	S3	8.1×10^{-7} (m)
μ_{peak}	0.66 ± 0.15	all	—
Ω_0	1.79 ± 0.38	S1A	4.37×10^{-7} (m sec)
Ω_0	1.66 ± 0.38	S1B	4.01×10^{-7} (m sec)
Ω_0	3.16 ± 0.09	S2	3.38×10^{-6} (m sec)
Ω_0	1.96 ± 0.02	S3	8.83×10^{-6} (m sec)
Ω_0	2.07 ± 0.16	all	—

within 25% of the actual yield. The difference between the two is less than the standard error associated with observational uncertainty and implies that the DM-based relation between i_{area} and R is applicable for large R values. This supports the idea that i_{area} is the most robust airblast observable and that propagation effects are subordinate to source effects even as the airblast enters the elastic regime.

The t_{dur} estimate is slightly less accurate, underpredicting the actual yield by about 35%. The observational uncertainties are relatively small and do not allow for overlap with the actual yield, thus the DM-based relation between T_{dur} and

R may not be strictly valid to large R . Nevertheless, the t_{dur} estimate is still of the same order of the actual yield and therefore is useful.

The least-accurate yield estimate is produced with the p_{peak} observation, which gives a value about 10 times as big as expected. Observational uncertainties lead to large enough errors that the estimate overlaps with the actual yield; however, their large magnitude renders p_{peak} inferior to t_{dur} and i_{area} as a yield estimator at least at near-elastic ranges.

Owing to the fact that the seismometers are capable of accurately recording airblast travel times, we have four σ observations for DB07 even though only a single pressure gauge was deployed. We report the multistation yield estimate in Table 5. The estimate is twice as large as the actual yield; however the error bounds overlap with the theoretical value.

We perform four single-station σ -based yields to facilitate a comparison with the other airblast observables (Table 5). Only station 3, with a scaled range of approximately 110 m, provides an estimate that is comparable in quality to those based on i_{area} and t_{dur} . The estimate from station 2, with R approximately 330 m, is comparable in quality to the p_{peak} estimate; however, the estimates as the furthest stations are off by two orders of magnitude. Clearly σ is most relevant as a yield estimator at small R , when the airblast is significantly shocklike and can only be used to provide upper bounds on the yield at near-elastic, large R ranges.

We made observations of μ_{peak} and Ω_0 for each of the four seismic stations, using the procedures described previously, and calculated multistation yield estimates using the DM functional relations (Table 5). The DB07 shot was in the same general area as the DM shots, and so we use equivalent solid earth properties, $\rho = 1.6 \text{ g/cm}^3$ and $\alpha = 1.0 \text{ km/sec}$, as used in deriving the DM relations. We calculated standard errors assuming observational uncertainties of 5.0 m in r , 5.0×10^{-9} m in μ_{peak} , and 1.0×10^{-7} m-sec in Ω_0 . Similar to the airblast properties, the dimensionless yield at stations S1A and S1B, $\Psi \approx 7 \times 10^{-13}$, is outside of the bounds that define the DM relations, $10^{-11} < \Psi < 10^{-8.5}$, and so extra uncertainty is added.

The multistation μ_{peak} yield estimate is virtually identical to the actual yield and has very small error associated with observational uncertainty. We performed four single station μ_{peak} based yield estimates as well and found little variation and no systematic trend in the values (Table 5). We infer that μ_{peak} has great value as a yield estimator even for lone stations with very small dimensionless yields and that the truck bomb-derived functional relation between Δ and Ψ can be applied to uncontained, surface chemical explosions.

The multistation Ω_0 yield overestimates the actual yield by a factor of 3 and has modest errors associated with observational uncertainty. We performed four single-station yield estimates as well and found values comparable to the multistation estimate with the two most-distant stations per-

forming the best. The systematic yield overestimation may reflect subtle Earth structure differences between the DM and DB07 sites that are unaccounted for in our truncated scaling laws. For example, at the DB07 site the water table is encountered at 20–30 m, much shallower than the 70–80 m depth for the DM site (Weir, 1965). This may cause more energy to be trapped near the surface for the DB07 experiment and explain the abnormally large Ω_0 values. Nevertheless the consistency of the single-station yield estimates implies that Ω_0 is robust as yield estimator even though it may be less portable than μ_{peak} .

The Nairobi Attack. On 7 August 1998 terrorists detonated a truck bomb at the U.S. embassy in Nairobi, Kenya, causing widespread damage and loss of life (Crowe *et al.*, 1999). The blast was recorded by a broadband seismometer located about 3 km northwest of ground zero (Hollnack and Schlüter, 1999). Previously, we performed a time-domain waveform inversion of the Nairobi seismic data for the geologic structure beneath downtown Nairobi, the origin time of the blast, and the seismic moment of the blast (Koper *et al.*, 1999). Because of trade-offs among the model parameters the moment could not be estimated precisely, and we found the range of acceptable values to be $1\text{--}8 \times 10^8 \text{ N m}$. Based on a preliminary analysis of the DM data we chose 3% as the seismic efficiency and so estimated the yield to be about $3 \times 10^3 \text{ kg TNT}$.

We can now estimate the Nairobi yield more simply and more accurately by using the DM-based scaling laws. The three applicable observables for yield estimation based on seismic data alone are σ , μ_{peak} , and Ω_0 . We list the values of these parameters for the Nairobi blast in Table 6 along with estimates of observational uncertainties. We perform single-station yield estimates with the DM relations and generate standard errors with the bootstrap technique (Table 6). We assume that the effective source properties in Nairobi are equivalent to those at the DM site.

For the σ -based estimate, the observational uncertainties are primarily due to origin time uncertainty and are large enough that a lower bound on the yield cannot be determined. We determine an upper bound of $3.3 \times 10^3 \text{ kg TNT}$ by considering the maximum likely value for σ . This bound is substantially lower than that reported in Koper *et al.* (1999) because the DM functional relation is used in lieu of the reference relation (equation 16 instead of equation 15) and the two approach slightly different values as R gets large. In any case, the yield constraint is still relatively weak

Table 6
Nairobi Yields from DM Relations

Waveform Property	Value	Observational Uncertainty Used	Yield, 10^3 kg TNT
Σ , m/sec	341.6	4.3	<3.32
μ_{peak} , m	6.7×10^{-7}	5.0×10^{-8}	5.73 ± 0.45
Ω_0 , m-sec	2.4×10^{-6}	5.0×10^{-7}	2.37 ± 0.46

because Σ quickly becomes essentially independent of R . We emphasize that the reported bound of 3.3×10^3 kg TNT applies to observational uncertainties only and does not account for uncertainties in the functional relation.

The Ω_0 yield of 2.4×10^3 kg TNT is consistent with the σ bound. However, the μ_{peak} yield is approximately twice as large, and the errors associated with observational uncertainties do not allow for overlap. The difference between the two seismic yield estimates is probably related to differences in near-source properties or along-path anelastic structure between the Nairobi and White Sands blast sites. Nevertheless the three scaling law estimates agree within a factor of about 2 and are consistent with the time-domain estimate of Koper *et al.* (1999).

Conclusions

The joint effort between the BATF and DTRA in conducting the Dipole Might test series has resulted in a unique and valuable data set for forensic seismologists. Based on the seismic and acoustic waveforms from the DM experiments, we have developed functional relations between several waveform properties and explosive mass. These relations can be used with appropriate scaling laws to perform yield estimation on data from uncontrolled explosions. In the case of average shock velocity and peak overpressure the functional relations we find are similar to previously defined reference curves. However, our relations for impulse per unit area and pulse duration are a significant improvement.

With respect to yield estimation, the most reliable and accurate acoustic waveform property is the impulse per unit area delivered by the airblast. This easy-to-measure property is effective up to relatively large scaled distances (900 m) and is extremely well correlated with yield. The second most reliable acoustic yield indicator is pulse duration. This feature is well correlated with yield and, similar to impulse per unit area, does not depend on an absolute timescale and therefore is insensitive to origin-time uncertainties. The peak overpressure and travel time of the airblast can also place helpful constraints on yield estimates but are less precise because of greater observational uncertainties and increased susceptibility to atmospheric inhomogeneities such as thermal gradients and wind.

Of the seismic waveform properties that were tested as yield estimators, we find that the peak amplitude of the initial P wave and the low-frequency asymptote of the displacement spectrum perform well. In contrast, the corner frequency is not suited for yield estimation over the range of normalized yields appropriate for truck bombings. The two effective seismic properties rival the best acoustic property for correlation with yield but the corresponding functional relations are probably less transportable owing to the complexity of shallow Earth structure compared to near-surface atmospheric structure. We note that seismometers are in general capable of recording the arrival time of the *airblast* with high accuracy, therefore, there are three independent func-

tional relations that can be used for yield estimation when only seismic data are available.

Our tests of the DM-derived functional relations on data from a non-truck bomb explosion indicate that they are applicable to surface chemical explosions in general and not limited solely to vehicle bomb explosions. Furthermore, the application of the DM relations to seismic data from the Nairobi bombing of 1998 gives consistent yield estimates of $2 - 6 \times 10^3$ kg TNT. In general our methodology provides for a quick, simple yield estimate of a surface chemical explosion when either seismic or acoustic data from a nearby (<10–20 km depending on the size of the explosion) receiver are available. Such source information is often important to investigative agencies whether the explosion in question resulted from a terrorist attack or an industrial accident.

Acknowledgments

We thank Dave Shatzer of the Bureau of Alcohol, Tobacco, and Firearms, and Matt Hossley of the U.S. Army Engineer Research and Development Center for their encouragement and permission to publish this work. We are grateful for the support received from Paul DeRego, Mark Drabecki, and James Harding of the DTRA Albuquerque office while conducting these experiments. Robert Martinez of DTRA assisted in the fielding of the DM 30 seismoacoustic experiment. Brian Stump and Anton Dainty provided critical reviews that significantly improved this article.

References

- Barker, T. G., K. L. McLaughlin, and J. Bonner (1997). Physical mechanisms of quarry blast sources (SSA meeting abstract), *Seism. Res. Lett.* **68**, 305–306.
- Bedard, A. J. Jr., and T. M. Georges (2000). Atmospheric infrasound, *Physics Today* **53**, 32–37.
- Chael, E. P., and R. E. Spalding (1996). Seismic signals from a bolide in Ecuador (supplement), *EOS* **77**, f508.
- Coppens, A. B., and R. A. Reinhardt (1993). *Explosives and Explosions*, Naval Postgraduate School, Monterey, California.
- Crowe, W. J., M. H. Armacost, P. C. Wilcox Jr., J. E. Nelson, A. W. Donahue, R. C. Brown, T. A. Todman, D. Busby, L. E. Davis, M. L. Rogers, and K. R. McKune (1999). *Report of the Accountability Review Boards, Bombings of the US Embassies in Nairobi, Kenya and Dar es Salaam, Tanzania on August 7, 1998*, U.S. Dept. of State, Washington, D.C.
- Denny, M. D., and L. R. Johnson (1991). The explosion seismic source function: models and scaling laws reviewed, in *Explosion Source Phenomenology*, American Geophysical Monograph 65, 1–24.
- DeRego, P. (1997). *Dipole Might 21 & 23*, Quick Look Data Report, Field Command, Defense Special Weapons Agency, Kirtland AFB, New Mexico.
- Evers, L. G., and H. W. Haak (2000). Seismo-akoestische analyse van de explosies bij S. E. Fireworks Enschede, 13 mei 2000, technical report, Koninklijk Nederlands Meteorologisch Instituut, Sectie Seismologie, September, 2000.
- Evers, L. G., and H. W. Haak (2001). Listening to sounds from an exploding meteor and oceanic waves, *Geophys. Res. Lett.* **28**, 41–44.
- General Electric Company–Tempo (1977). *Proceedings of the Dice Throw Symposium 21–23 June 1977*, Defense Nuclear Agency, Washington, D.C.
- Gupta, I. N., and R. R. Blandford (1983). A mechanism for generation of short-period transverse motion from explosions, *Bull. Seism. Soc. Am.* **73**, 571–591.

- Hollnack, D., and T. Schlüter (1999). A seismological evaluation of the Nairobi bomb blast of 7 August 1998, Bulletin UNESCO Nairobi Office, no. 33, 18–19.
- Holzer, T. L., J. B. Fletcher, G. S. Fuis, T. Ryberg, T. M. Brocher, and C. M. Dietel (1996). Seismograms offer insight into Oklahoma City bombing, *EOS* **77**, 393, 398–399.
- Ichinose, G. A., K. D. Smith, and J. G. Anderson (1999). Seismic analysis of the 7 January 1998 chemical plant explosion at Kean Canyon, Nevada, *Bull. Seism. Soc. Am.* **89**, 938–945.
- Kanamori, H., J. Mori, D. L. Anderson, and T. H. Heaton (1991). Seismic excitation by the space shuttle Columbia, *Nature* **349**, 781–782.
- Kedar, S., B. Sturtevant, and H. Kanamori (1996). The origin of harmonic tremor at Old Faithful Geyser, *Nature* **379**, 708–711.
- Kinney, G. F., and K. J. Graham (1985). *Explosive Shocks in Air*, Second Ed., Springer-Verlag, New York.
- Kitov, I. O., J. R. Murphy, O. P. Kusnetsov, B. W. Barker, and N. I. Nedoshivin (1997). An analysis of seismic and acoustic signals measured from a series of atmospheric and near-surface explosions, *Bull. Seism. Soc. Am.* **87**, 1553–1562.
- Koper, K. D., T. C. Wallace, and D. Hollnack (1999). Seismic analysis of the 7 August 1998 truck-bomb blast at the American Embassy in Nairobi Kenya, *Seism. Res. Lett.* **70**, 512–521.
- Lamb, F. K., B. W. Callen, and J. D. Sullivan (1991). Yield estimation using shock wave methods, in *Explosion Source Phenomenology*, American Geophysical Monograph 65, 73–89.
- McCormack, D. A., J. Drysdale, and A. L. Bent (1999). *A Seismological Perspective on the Crash of Swiss Air Flight 111 Near Halifax, Nova Scotia on 3 September 1998*, presented at 11th Annual IRIS Workshop, Fish Camp, California.
- Murphy, J. R. (1981). Near-field Rayleigh waves from surface explosions, *Bull. Seism. Soc. Am.* **71**, 223–248.
- Murphy, J. R., and H. K. Shah (1988). An analysis of the effects of site geology on the characteristics of near-field Rayleigh waves, *Bull. Seism. Soc. Am.* **78**, 64–82.
- Pechmann, J. C., W. R. Walter, S. J. Nava, and W. J. Arabasz (1995). The February 3, 1995, M_L 5.1 seismic event in the Trona mining district of southwestern Wyoming, *Seism. Res. Lett.* **66**, 25–34.
- Persson, P. A., R. Holmberg, and J. Lee (1994). *Rock Blasting and Explosive Engineering*, CRC Press, Boca Raton, Florida, 540 pp.
- Reinke, R. E. (1981). *Results of Seismic Surveys and Drilling for Mill Race Test Site Selection*, Appendix G-1 in Test Execution Report, MISTY CASTLE Series, MILL RACE Event, POR 7072, Defense Nuclear Agency, Kirtland AFB, New Mexico.
- Reinke, R. E. (1985). *A Digital Microbarograph System*, AFWL TR 84-142, Air Force Weapons Laboratory.
- Sadwin, L., and J. Pittman (1969). *Airblast Characterization of ANFO, Phase I*, TR 69-82, Naval Ordnance Laboratory, College Park, Maryland.
- Stump, B. W., and R. E. Reinke (1991). Free-field surface ground motions from nuclear explosions, their spatial variations, and the constraint of physical source mechanisms, in *Explosion Source Phenomenology*, Geophysical Monograph 65, AGU, Washington, DC, 47–61.
- Stump, B. W., D. C. Pearson, and R. E. Reinke (1999). Source comparisons between nuclear and chemical explosions detonated at Rainier Mesa, Nevada Test Site, *Bull. Seism. Soc. Am.* **89**, 409–422.
- Uhrhammer, R. A. (1996). Yosemite rock fall of July 10, 1996, *Seism. Res. Lett.* **67**, 47–48.
- Weir, J. E. Jr. (1965). Geology and availability of ground water in the northern part of White Sands Missile Range and vicinity of New Mexico, *U.S. Geol. Surv. Water Supply Paper 1801*.
- Yang, X., B. W. Stump, and P. W. Scott (1998). Source mechanism of an explosively induced mine collapse, *Bull. Seism. Soc. Am.* **88**, 843–854.
- Saint Louis University
St. Louis, Missouri 63103
(K.D.K.)
- University of Arizona
Tucson, Arizona, 85721
(T.C.W.)
- Defense Threat Reduction Agency
Kirtland Air Force Base, New Mexico, 87117
(R.E.R., J.A.L.)

Manuscript received 20 September 2000.